THE JOURNAL OF BIOLOGICAL CHEMISTRY VOL. 290, NO. 6, pp. 3693–3707, February 6, 2015
Published in the U.S.A.

# Matrix Metalloproteinase-14 Both Sheds Cell Surface Neuronal Glial Antigen 2 (NG2) Proteoglycan on Macrophages and Governs the Response to Peripheral Nerve Injury*

Received for publication, August 7, 2014, and in revised form, December 4, 2014 Published, JBC Papers in Press, December 8, 2014, DOI 10.1074/jbc.M114.603431

**Tasuku Nishihara**[‡§¶], **Albert G. Remacle**[‖], **Mila Angert**[‡§], **Igor Shubayev**[§], **Sergey A. Shiryaev**[‖], **Huaqing Liu**[‡§], **Jennifer Dolkas**[‡§], **Andrei V. Chernov**[‖], **Alex Y. Strongin**[‖], **and Veronica I. Shubayev**[‡§1]

*From the* [‡]*Departments of Anesthesiology, University of California, San Diego, La Jolla, California 92093,* [§]*Veterans Affairs San Diego Healthcare System, La Jolla, California 92037,* [‖]*Sanford-Burnham Medical Research Institute, La Jolla, California 92037, and* [¶]*Department of Anesthesiology and Resuscitology, Ehime University, Toon, Ehime 791-0295, Japan*

**Background:** In the nervous system, NG2, an integral membrane chondroitin sulfate proteoglycan, is expressed by macrophages and progenitor glia.
**Results:** Both NG2 shedding and axonal growth depend on the pericellular remodeling executed by MT1-MMP/MMP-14.
**Conclusion:** MT1-MMP inhibition restores sensory axon regeneration and attenuates hypersensitivity caused by peripheral nerve injury.
**Significance:** Our findings identify MT1-MMP as a novel therapeutic target in PNS injury and pain.

**Neuronal glial antigen 2 (NG2) is an integral membrane chondroitin sulfate proteoglycan expressed by vascular pericytes, macrophages (NG2-Mϕ), and progenitor glia of the nervous system. Herein, we revealed that NG2 shedding and axonal growth, either independently or jointly, depended on the pericellular remodeling events executed by membrane-type 1 matrix metalloproteinase (MT1-MMP/MMP-14). Using purified NG2 ectodomain constructs, individual MMPs, and primary NG2-Mϕ cultures, we demonstrated for the first time that MMP-14 performed as an efficient and unconventional NG2 sheddase and that NG2-Mϕ infiltrated into the damaged peripheral nervous system. We then characterized the spatiotemporal relationships among MMP-14, MMP-2, and tissue inhibitor of metalloproteinases-2 in sciatic nerve. Tissue inhibitor of metalloproteinases-2-free MMP-14 was observed in the primary Schwann cell cultures using the inhibitory hydroxamate warhead-based MP-3653 fluorescent reporter. In teased nerve fibers, MMP-14 translocated postinjury toward the nodes of Ranvier and its substrates, laminin and NG2. Inhibition of MMP-14 activity using the selective, function-blocking DX2400 human monoclonal antibody increased the levels of regeneration-associated factors, including laminin, growth-associated protein 43, and cAMP-dependent transcription factor 3, thereby promoting sensory axon regeneration after nerve crush. Concomitantly, DX2400 therapy attenuated mechanical hypersensitivity associated with nerve crush in rats. Together, our findings describe a new model in which MMP-14 proteolysis regulates the extracellular milieu and presents a novel therapeutic target in the damaged peripheral nervous system and neuropathic pain.**

Injury to axons in the peripheral nervous system (PNS)[2] normally reactivates an intrinsic regenerative program that enables a permissive extracellular matrix milieu enriched in laminin, fibronectin, and other growth-promoting factors (1). In turn, secreted and extracellular matrix-bound chondroitin sulfate proteoglycans (CSPGs) typically form inhibitory gradients for axonal growth (2, 3).

CSPG-4/neuronal glial antigen 2 (NG2) is a structurally and functionally unique integral membrane proteoglycan (4). In the central nervous system (CNS), NG2 is expressed by the cycling, NG2-expressing glial progenitor cells (henceforth termed NG2-glia) and pericytes (4), whereas in the PNS, fibroblast-like cells and pericytes are the main cell sources of NG2 (5, 6). Because of its direct interactions with extracellular matrix proteins and adhesion receptors, NG2 governs cell proliferation and migration (7). Moreover, hematogenous macrophages (Mϕ) expressing NG2 (henceforth termed NG2-Mϕ) infiltrate the damaged CNS (8–14). Although the specific functions of the Mϕ subpopulation and their distinction from microglial functions in the CNS are still debated, strong support exists for neuroprotective properties of NG2-Mϕ in the CNS (12–15). Herein, we provide the first evidence that NG2-Mϕ infiltrate the PNS postinjury.

* This work was supported, in whole or in part, by National Institutes of Health Grants RO1DE022757 (to V. I. S. and A. Y. S.) and UL1 RR031980 (to University of California, San Diego and A. G. R.). This work was also supported by Department of Veterans Affairs Grant 5IO1BX000638 (to V. I. S.).

[1] To whom correspondence should be addressed: Dept. of Anesthesiology, University of California, San Diego, 9500 Gilman Dr., La Jolla, CA 92093-0629. Tel.: 858-534-5278; Fax: 858-534-1445; E-mail: vshubayev@ucsd.edu.

[2] The abbreviations used are: PNS, peripheral nervous system; ATF3, cAMP-dependent transcription factor 3; CSPG, chondroitin sulfate proteoglycan; MT1-MMP, membrane-type 1 matrix metalloproteinase; Mϕ, macrophages; NG2, neuronal glial antigen 2; TIMP, tissue inhibitor of metalloproteinases; GAP-43, growth-associated protein 43; TBI, traumatic brain injury; PFA, paraformaldehyde; DRG, dorsal root ganglia; L, lumbar; EC, ectodomain; qPCR, quantitative PCR.

Pericellular proteolysis by the membrane-type (MT) and soluble proteinases of the matrix metalloproteinase (MMP) family, including collagenases, gelatinases, and stromelysins, regulates the levels and biological functions of the extracellular matrix and cell membrane proteins (16, 17), including NG2 (18). Tissue inhibitors of metalloproteinases (TIMPs) control the cleavage activity of MMPs. In contrast with other MMPs, ubiquitous MMP-14/MT1-MMP, the proinvasive proteinase in many cancer types, is not inhibited by TIMP-1. Accordingly, inhibition of NG2 cleavage by TIMP-2 and -3, but not by TIMP-1, favors the role of MMP-14 in this proteolytic process (18).

MMPs play diverse roles in PNS repair. The broad spectrum inhibition of the catalytic MMP activity immediately after PNS injury helps to enhance the rate of sensory axonal regeneration by both promoting Schwann cell mitosis (19) and limiting the extent of myelin and axon damage, which are sequentially controlled by gelatinases B (MMP-9) and A (MMP-2) (19–24). MMP-2, however, also has a capacity to promote axonal growth in the PNS *ex vivo* through degradation of CSPGs (25, 26). It is possible that MMP-2 plays a potentially beneficial role in nerve repair. However, the high homology of the MMP-2 and MMP-9 gelatinases limits their selective pharmacological targeting. Conversely, targeting of the upstream regulator of pro-MMP-2 activation, MMP-14, represents a valuable alternative. Studies of MMP-14 in the PNS have thus far been limited to the evidence of its gene expression (20, 27).

Here, using purified proteins and primary NG2-M$\phi$ cultures, we have demonstrated for the first time that MMP-14 is a major NG2 sheddase. Because short term local inhibition of MMP-14 with a selective, function-blocking antibody enhanced sensory axon regeneration, MMP-14 appears to be a key, functionally relevant protease in injured sciatic nerve and a promising drug target in PNS postinjury.

## EXPERIMENTAL PROCEDURES

### *Reagents and Antibodies*

Routine reagents were purchased from Sigma unless indicated otherwise. The broad spectrum hydroxamate inhibitor (GM6001) was from EMD Millipore. The function-blocking fully human MMP-14 antibody (DX2400) was kindly provided by Dyax (Burlington, MA) (28). Human IgG1 control was obtained from Abcam. The following antibodies were also used in our experiments: rabbit polyclonal S100 antibody (Z0311, Dako), murine monoclonal CD68 antibody (MCA341R, Serotec), rabbit polyclonal Iba1 antibody (019-19741, Wako), rabbit polyclonal laminin antibody (L9393, Sigma), murine monoclonal $\beta$-actin antibody (A53166, Sigma), and rabbit polyclonal TIMP-2 antibody (C0348, Assay Biotechnology). Murine monoclonal and rabbit polyclonal MMP-14 antibodies (3G4/MAB1767 and AB8345, respectively), murine monoclonal MMP-2 antibody (MAB3308), rabbit polyclonal NG2 antibody (AB5320), and rabbit polyclonal growth-associated protein 43 (GAP-43; AB5220) antibody were purchased from EMD Millipore.

### *MMPs and TIMP-2*

The individual catalytic domain of MMP-14 was expressed in *Escherichia coli* and purified from the inclusion bodies in 8 M urea using metal-chelating chromatography (29). The purified MMP-14 samples were then refolded to restore their native conformation and proteolytic activity. The recombinant pro forms of MMP-2 and MMP-9 were purified from the serum-free medium conditioned by the stably transfected human embryonic kidney 293 cells using gelatin-Sepharose chromatography. Pro-MMP-2 and pro-MMP-9 were activated using 4-aminophenylmercuric acetate as described earlier (30). The purity of the isolated MMPs was confirmed by SDS-polyacrylamide gel electrophoresis followed by Coomassie staining of the gels. Only the samples in which the level of purity exceeded 95% were used in our studies. The concentration of the catalytically active MMPs was measured using a fluorescence assay by titration against a standard GM6001 solution of known concentration. (7-Methoxycoumarin-4-yl)acetyl-Pro-Leu-Gly-Leu-(3-[2,4-dinitrophenyl]-L-2,3-diaminopropionyl)-Ala-Arg-$NH_2$ (Bachem) was used as a fluorescent substrate. The steady-state rate of the substrate cleavage by MMP was plotted as a function of inhibitor concentration and fitted with the following equation: $V = \mathrm{SA}(E_0 - 0.5\{(E_0 + I + K_i) - [(E_0 + I + K_i)^2 - 4E_0I]^{0.5}\})$ where $V$ is the steady-state rate of substrate hydrolysis, SA is specific activity (rate per unit of enzyme concentration), $E_0$ is enzyme concentration, $I$ is inhibitor concentration, and $K_i$ is the dissociation constant of the enzyme·inhibitor complex (31). The activated MMPs were used immediately in our assays. Recombinant human TIMP-2 was expressed in Madin-Darby canine kidney cells and purified from conditioned medium as reported earlier (32).

### *Animal Models and Therapy*

All animal procedures were performed according to the Public Health Service Policy on Humane Care and Use of Laboratory Animals, and the protocol was approved by the Institutional Animal Care and Use Committee at the Veterans Affairs San Diego Healthcare System. Animals were gender- and age-matched and randomly assigned to the experimental groups. Sprague-Dawley 8–10-week-old female or male (for NG2-M$\phi$ cultures only) rats (Harlan) were housed in plastic cages at ambient temperature on a 12-h light-dark cycle with free access to food and water. Anesthesia was achieved with 4% isoflurane (Isothesia, Henry Schein) in 55% oxygen.

*Traumatic Brain Injury (TBI)*—TBI was done as described previously (12). Following a 15-mm longitudinal incision in the skull, through two holes made ~2.5 and ~4 mm to the right of the midline and 1 mm posterior to bregma, a sterile 26-gauge needle was inserted to ~7-mm depth and moved in a fanlike manner parallel to the midline.

*Sciatic Nerve Crush*—Sciatic nerve crush was performed in the sciatic nerve exposed unilaterally at the midthigh level through a gluteal muscle-splitting incision (19). Nerve crush was accomplished using smooth surface forceps twice for 2 s each. The lesion site was labeled using a 6-0 nylon suture to the adjacent muscle. Where indicated, DX2400 (1.13 mg/ml; corresponding to ~22 $\mu$g/kg), control IgG1 (1.13 mg/ml), or vehicle (PBS, Steris Labs) was administered intraneurally into the sciatic nerve fascicle in a 5-$\mu$l volume at day 3 postcrush using a 33-gauge needle. Animals were perfused transcardially using 4% paraformaldehyde (PFA) in 0.2 M phosphate buffer under deep anesthesia or sacrificed by intraperitoneal injection of

Euthasol (100–150 mg/ml; Virbac Animal Health). Tissues (brain, lumbar (L) 4 and L5 dorsal root ganglia (DRG), and sciatic nerve) were excised, snap frozen in liquid nitrogen, and stored at −80 °C or in the RNAlater reagent (Ambion) at −20 °C until use.

### Cells

*Primary NG2-Mϕ*—Primary NG2-Mϕ were prepared from TBI lesions (day 7) as described previously (12). The TBI-containing brain hemisphere tissues were minced in 0.02% EDTA in PBS, filtered using a nylon mesh (160 μm; EMD Millipore), and centrifuged at 4 °C (1,000 rpm for 5 min). The pellet was resuspended and incubated in a suspension culture dish (Sarstedt) in DMEM (Invitrogen) supplemented with 3% FBS for 30 min. Unattached debris and cells were removed by washing in 3% FBS in DMEM, and attached Mϕ were incubated for 30 min in E2 medium (serum-free DMEM containing 10 mM HEPES (pH 7.3), 4.5 mg/ml glucose, 5 μg/ml insulin, 5 μg/ml transferrin, 5 nM sodium selenite (insulin-transferrin-selenium, Invitrogen), and 0.2 mg/ml BSA (33). This procedure yielded >90% pure NG2-Mϕ cultures as confirmed by dual immunoreactivity for NG2 and CD68. Where indicated, cells were supplemented with MMP-14 (1 μg/ml), TIMP-2 (50 ng), or GM6001 (10 μM) for 30 min.

*Primary Schwann Cells*—Primary Schwann cells were isolated from sciatic nerves of postnatal day 1–3 Sprague-Dawley rats (34) and further purified from fibroblasts using the mitotic poison AraC (10 μM; not toxic to Schwann cell viability), an anti-fibronectin Thy1.1 antibody, and rabbit complement (24). Schwann cells were grown in DMEM, 10% FBS containing 21 μg/ml bovine pituitary extract and 4 μM forskolin. Schwann cell purity was confirmed by >95% immunoreactivity for S100. Schwann cells were passaged upon reaching confluence. Cells from passages 3–7 were collected and transferred into wells of a 6- or 12-well plate to grow for 16–24 h in DMEM, 10% FBS.

*Human Breast Carcinoma MCF7*—Human breast carcinoma MCF7 cells were obtained from ATCC (Manassas, VA) and cultured in DMEM, 10% FBS containing gentamicin (10 μg/ml). MCF7 cells stably transfected with the empty pcDNA3-zeo vector (MCF7-mock cells) or the pcDNA3-zeo plasmid encoding the full-length MMP-14 (MCF7-MMP14 cells) were described earlier (35).

### Recombinant Ectodomain Constructs of Rat NG2 and the NG2 Antibodies

The soluble recombinant non-glycosylated ectodomain fragments of rat NG2 used in our study were expressed and purified as described earlier (36) (see Fig. 1*A*). The full-length ectodomain (EC; amino acid residues 1–2223) and its truncation lacking the C-terminal portion of the D2 domain and the entire D3 domain (ECΔ3; residues 1–1465) were expressed in human embryonic kidney 293 cells and purified using a DEAE-Sepharose column. The purified fragments were then treated with chondroitinase ABC to remove the glycosaminoglycan chains. The D2 domain (residues 632–1450) and D3 domain (residues 1587–2218) constructs were C-terminally tagged with a $His_6$ tag, expressed in human embryonic kidney 293-EBNA cells and purified using a nickel-agarose column. The 293-EBNA cell line stably expressing the Epstein Barr Virus *EBNA-1* gene from pCMV/EBNA. Expression of the *EBNA-1* gene is controlled by the CMV promoter and is high-level and constitutive. The specificity of the five NG2 antibodies we used (which were directed against the individual portions of the NG2 ectodomain) was described earlier (37, 38). Thus, the rabbit polyclonal EC, D2, and D3 antibodies were raised against the purified individual EC, D2, and D3 domain constructs, respectively. The rabbit 1088 antibody was raised against a 19-residue peptide from the N-terminal portion of the D1 domain. The rabbit polyclonal 1657 antibody was raised against a 19-residue peptide from the C-terminal 2161–2179 sequence of the D3 domain. We also used the murine monoclonal 05-710 antibody (clone 132.38, EMD Millipore) raised against the recombinant D3 domain. The NG2 recombinant ectodomain constructs and the antibodies were a generous gift from Dr. William Stallcup (Sanford-Burnham Medical Research Institute, La Jolla, CA).

### In Vitro Cleavage of NG2 Constructs

Purified NG2 constructs (EC (2 μg; 0.4 μM), D2 (2 μg; 1 μM), D3 (2 μg; 1 μM), and ECΔ3 (2 μg; 0.65 μM)) were co-incubated for 1 h at 37 °C with MMP-2, MMP-9, or MMP-14 (1:10–1:100 enzyme-substrate molar ratio) in 20-μl reactions containing 50 mM HEPES, pH 6.8 supplemented with 10 mM $CaCl_2$ and 50 μM $ZnCl_2$. Where indicated, GM6001 (1 μM) was added to inhibit MMPs. The cleavage was stopped by adding 5× SDS sample buffer to the reactions. Aliquots of the digests were analyzed by SDS-gel electrophoresis in 3–8% gradient Tris-acetate gels (Invitrogen) followed by Coomassie staining (20-μl samples) and by immunoblotting (2-μl samples) with the EC, D2, D3, 1088, 1657, and 05-710 NG2 antibodies (dilution, 1:1,000 each).

### Imaging of the Catalytic Cell Surface MMP-14 Activity

Detection of the cellular MMP-14 activity was performed using the inhibitory hydroxamate warhead-based MP-3653 reporter synthesized as described previously (32). The MP-3653 reporter represents a liposome tagged with a fluorochrome and functionalized with a PEG chain spacer linked to a selective inhibitory hydroxamate warhead, thereby targeting the catalytically active membrane-tethered MMP-14 enzyme alone (32). Both the MMP-14 proenzyme and the stoichiometric MMP-14·TIMP-2 complex do not interact with MP-3653. Cells were plated in DMEM, 10% FBS medium on a 15-mm glass coverslip coated with poly-D-lysine (50 μg/ml) and allowed to reach 25–70% confluence. Cells were then washed with DMEM and incubated for 30 min at 37 °C in DMEM supplemented with 0.2% BSA alone or jointly with GM6001 (1 μM). Cells were next incubated for 3 h at 37 °C in DMEM, 0.2% BSA supplemented with the MP-3653 reporter (25 nM) alone or jointly with GM6001 (1 μM) followed by washing in PBS and fixation in 4% PFA. The slides were mounted in Vectashield medium containing DAPI and analyzed using a 20× objective on an Olympus BX51 fluorescence microscope equipped with a MagnaFire digital camera.

### Immunoblotting

Schwann cell lysates were prepared in TBS supplemented with 50 mM *N*-octyl β-D-glucopyranoside, 1 mM $CaCl_2$, 1 mM

**TABLE 1**

**Primer and probe sequences for TaqMan qPCR**

TaqMan probes contained the 5′-reporter *carboxyfluorescein (*FAM) and the 3′-quencher minor groove binder (MGB), Black Hole Quencher (BHQ)-1, or *4-(dimethylaminoazo)benzene-4-carboxylic acid (DABCYL)* dye. Primers and probes were obtained from Biosearch Technologies unless indicated otherwise. Roche, Roche Applied Science; AB, Applied Biosystems.

| Gene | GenBank™ accession no. | Sequences (5′–3′) |
|---|---|---|
| *MMP-14,* rat | NM_031056 | Forward, AACTTCGTGTTGCCTGATGA<br>Reverse, TTTGTGGGTGACCCTGACTT<br>Probe, Roche no. 42 (04688015001) |
| *MMP-2,* rat | NM_031054 | AB kit (Rn01538167_m1) |
| *TIMP-2,* rat | NM_021989 | Forward, CGTTTTGCAATGCAGACGTA<br>Reverse, GATGGGGTTGCCATAGATGT<br>Probe, Roche no. 10 (04685091001) |
| *ATF3,* rat | NM_012912 | Forward, TGTCAGTCACCAAGTCTGAGGT<br>Reverse, CACTTGGCAGCAGCAATTT<br>Probe, Roche no. 70 (04688937001) |
| *GAPDH,* rat | X02231 | Forward, GAACATCATCCCTGCATCCA<br>Reverse, CCAGTGAGCTTCCCGTTCA<br>Probe, CTTGCCCACAGCCTTGGCAGC |

$MgCl_2$, 1 mM phenylmethylsulfonyl fluoride, 10 mM EDTA, and protease inhibitor mixture set III. The crude nerve extracts and NG2-M$\phi$ lysates were prepared in TBS supplemented with 1% Triton X-100, 10% glycerol, 0.1% SDS, 5 mM EDTA, 1 mM phenylmethylsulfonyl fluoride, aprotinin, pepstatin, and leupeptin (1 $\mu$g/ml each). Insoluble material was removed by centrifugation (14,000 $\times$ *g* for 15 min). Extract aliquots (3–25 $\mu$g of total protein each) were separated by SDS-gel electrophoresis in either 4–12% gradient NuPAGE-MOPS gels (Invitrogen) or 7, 10, and 15% Tris-glycine gels (Bio-Rad). Separated proteins were then transferred onto a nitrocellulose or PVDF membrane. The membrane was blocked in 5% nonfat milk (Bio-Rad) and incubated for 16–18 h at 4 °C with the primary antibodies followed by incubation for 1 h at ambient temperature with the species-specific horseradish peroxidase-conjugated goat secondary antibody (Cell Signaling Technology; 1:10,000 dilution). The blots were developed using an enhanced chemiluminescence system (GE Healthcare) or a SuperSignal West Dura Extended Duration Substrate kit (Thermo Scientific). The membranes were reprobed using a $\beta$-actin antibody (loading control). The bands were digitized and quantitated using ImageJ.

### Gelatin Zymography

Schwann cells ($5 \times 10^5$) were grown in wells of a 12-well plate containing DMEM, 10% FBS supplemented with bovine pituitary extract (21 $\mu$g/ml) and forskolin (4 $\mu$M). In 24 h, cells were replenished with fresh serum-free medium (0.6 ml) and incubated for an additional 16–18 h. The status of MMP-2 in the conditioned medium aliquots (20 $\mu$l) was analyzed using a precast 10% acrylamide gel co-polymerized with 0.1% gelatin (Invitrogen). After electrophoresis, the gel was incubated at ambient temperature twice for 30 min in 2.5% Triton X-100 and then for 16–18 h at 37 °C in 50 mM Tris-HCl, pH 7.4 containing 10 mM $CaCl_2$, 1 $\mu$M $ZnCl_2$, and 0.02% $NaN_3$. The gel was stained with Coomassie Blue R-250 to visualize the bands with gelatinolytic activity.

### qPCR

The rat sciatic nerves and DRG were isolated and stored in RNAlater (Ambion) at −20 °C. Total RNA was extracted from Schwann cells or nerve tissues using TRIzol (Invitrogen) and purified on an RNeasy Mini column (Qiagen). The RNA purity was estimated by measuring the $A_{260/280}$ ratio. The samples were treated with RNase-free DNase I (Qiagen). cDNA was synthesized using a Transcriptor First Strand cDNA Synthesis kit (Roche Applied Science). Primers and TaqMan probes (Table 1) were obtained and optimized as described (24). Gene expression levels were measured in a Mx4000™ Multiplex Quantitative PCR System (Agilent Technologies) using 50 ng of cDNA and 2× TaqMan Universal PCR Master Mix (Ambion) with a one-step program: 95 °C, 10 min; 95 °C, 30 s; 60 °C, 1 min for 50 cycles. Duplicate samples without cDNA (a no template control) showed no contaminating DNA. Relative mRNA levels were quantified using the comparative ΔCt method (39), and glyceraldehyde-3-phosphate dehydrogenase (GAPDH) was used as a normalizer. The -fold change between experimental and control samples was determined using the Mx4000 software.

### Immunostaining

Schwann cells and NG2-M$\phi$ grown on a coverslip were washed with PBS, fixed in 4% PFA, and blocked for 1 h in 10% BSA. Tissues (brain and sciatic nerve) were excised, postfixed in 4% PFA, rinsed, cryoprotected in a 15–30% sucrose gradient, embedded into optimum cutting temperature compound (Sakura Finetek) in liquid nitrogen, and cut into 10-$\mu$m-thick sections. Teased nerve fibers were prepared from the separated nerve bundles using fine smooth microforceps and incubated in 5% fish skin gelatin and 0.1% Triton X-100 in PBS for 1 h. Nonspecific binding was blocked using 10% normal goat serum. The slides were incubated for 16–18 h at 4 °C with a primary antibody (specified above) followed by incubation for 1 h at ambient temperature with a species-specific secondary antibody conjugated with Alexa Fluor 488 (green) or Alexa Fluor 594 (red) (dilution, 1:200 each; Molecular Probes). After staining, individual fibers were teased out on a glass slide using a 0.20–0.22-mm acupuncture needle (Vinco, Oxford Medical Supplies) for observation. Slides were mounted using Vectashield medium containing DAPI or Slowfade Gold antifade reagent (Molecular Probes). Alternatively, biotin-conjugated secondary antibodies (Jackson ImmunoResearch Laboratories) followed by Vectastain Elite ABC System, 3′,3-diaminobenzidine substrate (Vector Laboratories), and methyl green counterstain

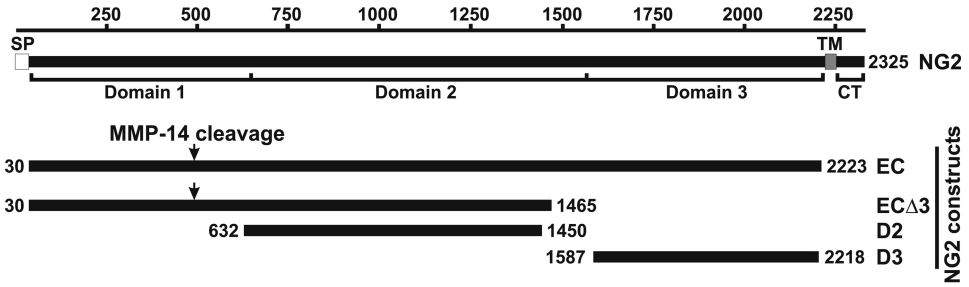


FIGURE 1. **Schematic representation of the domain structure of NG2 and the purified NG2 ectodomain fragments.** The residue numbering is shown at the *top*. *SP*, *TM*, and *CT*, the signal peptide, the transmembrane domain, and the cytoplasmic tail, respectively. *EC*, the full-length NG2 ectodomain; *EC*Δ*3*, the NG2 ectodomain lacking D3; *D2*, central domain 2 of NG2; *D3*, juxtamembrane domain 3 of NG2. The *numbers* at the *beginning* and *end* of each construct refer to the residue numbering. The *arrows* indicate the putative MMP-14 cleavage site in the D1 domain.

were used. Signal specificity was confirmed by omitting the primary antibody or by using the non-immune serum.

For morphometric analysis, the images were acquired using a Leica DMR microscope and Openlab 4.04 imaging software (Improvision) using a digital gain of ×1, the maximum white level, and an exposure time of 1 s and a black level of 283 for GAP-43, an exposure time of 1.5 s and a black level of 188 for laminin, and an exposure time of 2.0 s and a black level of 97 for NG2. Quantitation was done using ImageJ software in three randomly selected areas per section per $n$ ($n = 5$/group) by an investigator unaware of the animal groups.

### *Nerve Pinch Test*

Based on the anticipated speed of sciatic nerve regrowth, the rate of sensory axon regeneration is assessed using a nerve pinch test between 2 and 7 days after crush (19, 40, 41). Thus, at day 7 postcrush, the sciatic nerve and its tibial nerve branch were exposed in the lightly anesthetized rats. Consecutive 1-mm-long segments of the tibial nerve were pinched with a pair of fine forceps starting from the distal end of the nerve and proceeding in the proximal direction until a reflex response, such as contraction of the muscles of the back, was observed. The distance between the most distal point of the nerve that produced a reflex withdrawal response and the stitch marking the crush site was measured under a dissecting microscope and identified as the regeneration distance (see Fig. 7*C*).

### *von Frey Test*

Sensitivity to non-noxious mechanical stimuli was measured using a von Frey test using the up-and-down method (42) by an investigator unaware of the animal groups. Rats were acclimated to being on a suspended 6-mm wire grid for 5 days. The plantar surface of the hind paw within the sciatic nerve innervation area was stimulated using calibrated von Frey filaments (Stoelting) at baseline (days −5, −3, −1, and 0 postinjury) and days 3, 5, and 7 postinjury. Stimuli were applied for 2 s with a 0.4–15.0-g buckling force to the mid paw plantar surface with ascending filament stiffness until a paw withdrawal response occurred. Stimuli were separated by several-second intervals or until the animal was calm with both hind paws placed on the grid. The consecutive way of applying filaments was continued until six responses were recorded. The 50% threshold was calculated as described (42).

### *Statistics*

Data were analyzed using GraphPad Prism 6 (GraphPad Software). The results were expressed as mean ± S.E. A two-tailed Student's $t$ test was used for comparison of two groups. Analysis of variance with Bonferroni's post hoc test was used for comparison of three or more groups. The $p$ values below 0.05 were considered statistically significant.

## RESULTS

*MMP-14 Proteolysis of NG2 in Vitro*—The full-length membrane NG2 consists of a large ectodomain divided into three subdomains (the N-terminal globular domain 1 (D1), the central domain 2 (D2), and the juxtamembrane domain 3 (D3)) followed by a transmembrane domain and a cytoplasmic tail (Fig. 1). To determine their relative NG2 cleavage efficiency, the equivalent concentrations of the active site-titrated MMPs, including MMP-2, MMP-9, and MMP-14, were co-incubated with the purified non-glycosylated 1–2223 NG2 EC at enzyme-substrate molar ratios of 1:10 and 1:100. MMP-2 and MMP-9 proteolysis of the EC construct was exceedingly limited. In contrast, MMP-14 efficiently cleaved the EC construct and as a result, three (210-, 160-, and 51–52-kDa) major cleavage products were generated in the cleavage reactions (Fig. 2*A*).

Because MMPs normally cleave the C-terminal portion of NG2 according to previous data by others (18, 37, 43), we tested whether MMP-14 cleaved the similar region of NG2. For this purpose, we compared the proteolysis of the 1–2223 EC construct *versus* the 1–1465 ECΔ3 truncation lacking the C-terminal D3 domain. Fig. 2*B* shows that the 51–52-kDa cleavage fragment was present in both digests, suggesting that MMP-14 did not cleave within the C-terminal D3 moiety. Conversely, our data suggested that MMP-14 cleaved the N-terminal portion of NG2.

To additionally confirm the specificity of the NG2 antibodies we used, we performed immunoblotting with the 1088, D2, D3, and 05-710 antibodies against the intact 632–1450 D2 and 1587–2218 D3 domains. As we expected, the D2 antibody recognized the D2 domain, and the D3 and 05-710 antibodies recognized the D3 domain, whereas both the D2 and D3 domains were not recognized by the 1088 antibody that was raised against the N-terminal portion of NG2 (Fig. 2*C*). Taken together, these results suggested that the NG2 antibodies could be used to assign the domain specificity of the EC cleavage products.

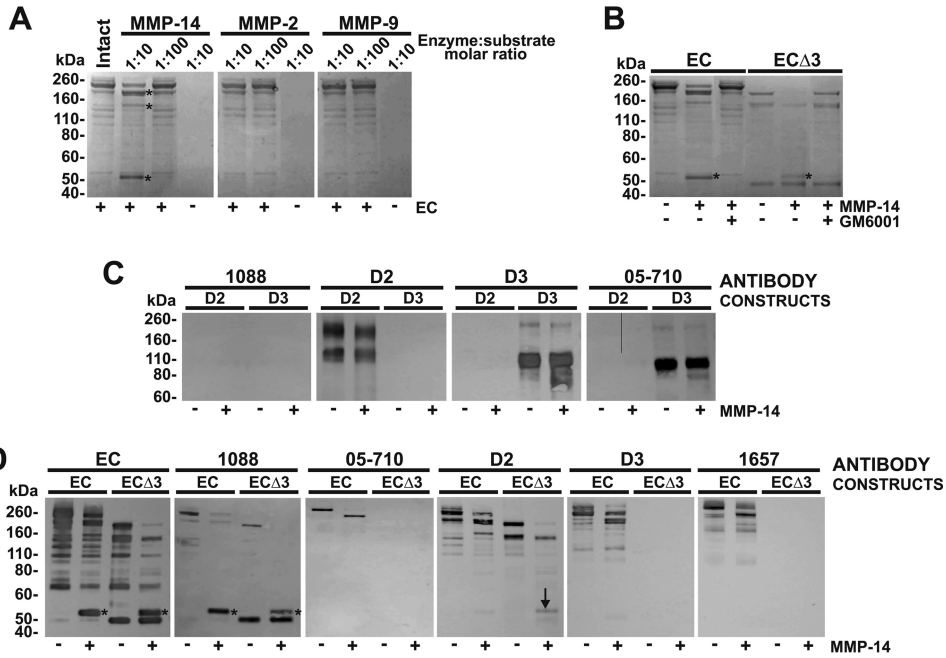


FIGURE 2. ***In vitro* cleavage of the purified NG2 ectodomain fragments by MMP-14.** *A*, cleavage of rat NG2 by MMP-2, MMP-9, and MMP-14. The proteases were co-incubated for 1 h at 37 °C with purified EC construct at the indicated enzyme-substrate molar ratio. The resulting cleavage products are shown by *asterisks*. *B*, the purified EC and ECΔ3 constructs were co-incubated for 1 h at 37 °C with MMP-14 at a 1:10 enzyme-substrate molar ratio. The digests were separated by SDS-gel electrophoresis followed by Coomassie staining. The ~51–52-kDa NG2 cleavage fragment is shown by an *asterisk*. Where indicated, GM6001 was added to the reactions. *C*, confirmation of the specificity of the NG2 antibodies. The D2 antibody recognized the intact D2 domain. The D3 and 05-710 antibodies recognized the intact D3 domain. The anti-D1 1088 antibody did not recognize the intact D2 and D3 domains. *D*, MMP-14 cleaves the N-terminal portion of NG2. The purified EC and ECΔ3 constructs were each co-incubated with MMP-14 at a 1:10 enzyme-substrate molar ratio. The digests were analyzed by immunoblotting using the indicated NG2 antibodies. The N-terminal ~51–52-kDa cleavage fragment is shown by an *asterisk*. The *vertical arrow* points to a nonspecific band.

To determine the cleavage fragment positions in the EC sequence, the purified EC construct and its ECΔ3 truncation were co-incubated with MMP-14. The digests were analyzed by immunoblotting with the antibodies against the individual D2 and D3 domains (Fig. 2*D*). The 51–52- and 210-kDa (and a corresponding 160-kDa fragment in ECΔ3) major cleavage fragments were detected in both EC and ECΔ3 digests. These results suggested that the major N-terminal 51–52-kDa and the C-terminal 210-kDa fragments of the EC construct originated due to MMP-14 proteolysis in the N-terminal D1 domain sequence.

*The MMP-14/MMP-2/TIMP-2 Axis in the PNS*—MMP-14 activity is required for the activation of the latent MMP-2 proenzyme (44). Both MMP-14 activity and MMP-2 activation are regulated by TIMP-2, which forms a stable, stoichiometric 1:1 complex with both MMP-14 and the MMP-2 proenzyme. In sciatic nerve, activated MMP-2 enzyme is observed at day 3 postinjury (22). We analyzed the changes in MMP-14 and concurrently MMP-2 and TIMP-2 in the sciatic nerve samples obtained at day 0 (normal) and days 1, 3, and 7 after crush injury.

The MMP-14 immunoreactivity and mRNA and protein levels in the normal nerve were low (Fig. 3, *A–C*). The protease appeared to be predominantly associated with the endothelial cells of the blood vessels and in crescent-shaped Schwann cells (Fig. 3*A*). There was a gradual increase in MMP-14 after nerve injury. In addition to the endothelial cells, MMP-14 was elevated, especially at days 3 and 7, in crescent-shaped, S100-positive Schwann cells (Fig. 3, *A* and *D*) and in Iba1-positive Mϕ (Fig. 3, *A*, *day 3*, *inset*, and *D*). In the majority of endoneurial cells, including Schwann cells, the MMP-14 immunoreactivity co-localized with TIMP-2 (Fig. 3*E*, *white arrows*), although MMP-14-positive but TIMP-2-negative areas were also recorded (Fig. 3*E*, *yellow arrows*).

According to the qPCR data, there was a mild decrease in the mRNA levels of MMP-14, MMP-2, and TIMP-2 at day 1 postcrush followed by a rapid and continuous increase of these three mRNA species between days 3 and 7 (Fig. 3*B*). Immunoblotting of the nerve lysate samples corroborated the qPCR results (Fig. 3*C*). Thus, the levels of MMP-2 and MMP-14 significantly increased at days 3–7 postinjury compared with day 0. In contrast with normal nerve, the active, 68-kDa MMP-2 enzyme was detected in the day 3 and especially day 7 samples. High levels of TIMP-2 (21 kDa) observed throughout the time course, including normal nerve, were not significantly different especially if calculated relative to β-actin (Fig. 3*C*). Together, the levels of MMP-2 and MMP-14 likely exceeded the levels of TIMP-2 protein only at days 3–7 postcrush.

Together, these novel findings indicated an elevated expression of MMP-14 and its inhibitor, TIMP-2, in Schwann cells, endothelial cells, and Mϕ in the injured PNS. High levels of TIMP-2 at day 0 implies that MMP-14 activity is tightly controlled in the adult normal nerve and that this inhibitory control of MMP-14 activity becomes misbalanced following injury, leading as a result to both the presence of MMP-14 unencumbered by TIMP-2 and a considerable level of MMP-2 activation at days 3–7 postcrush.

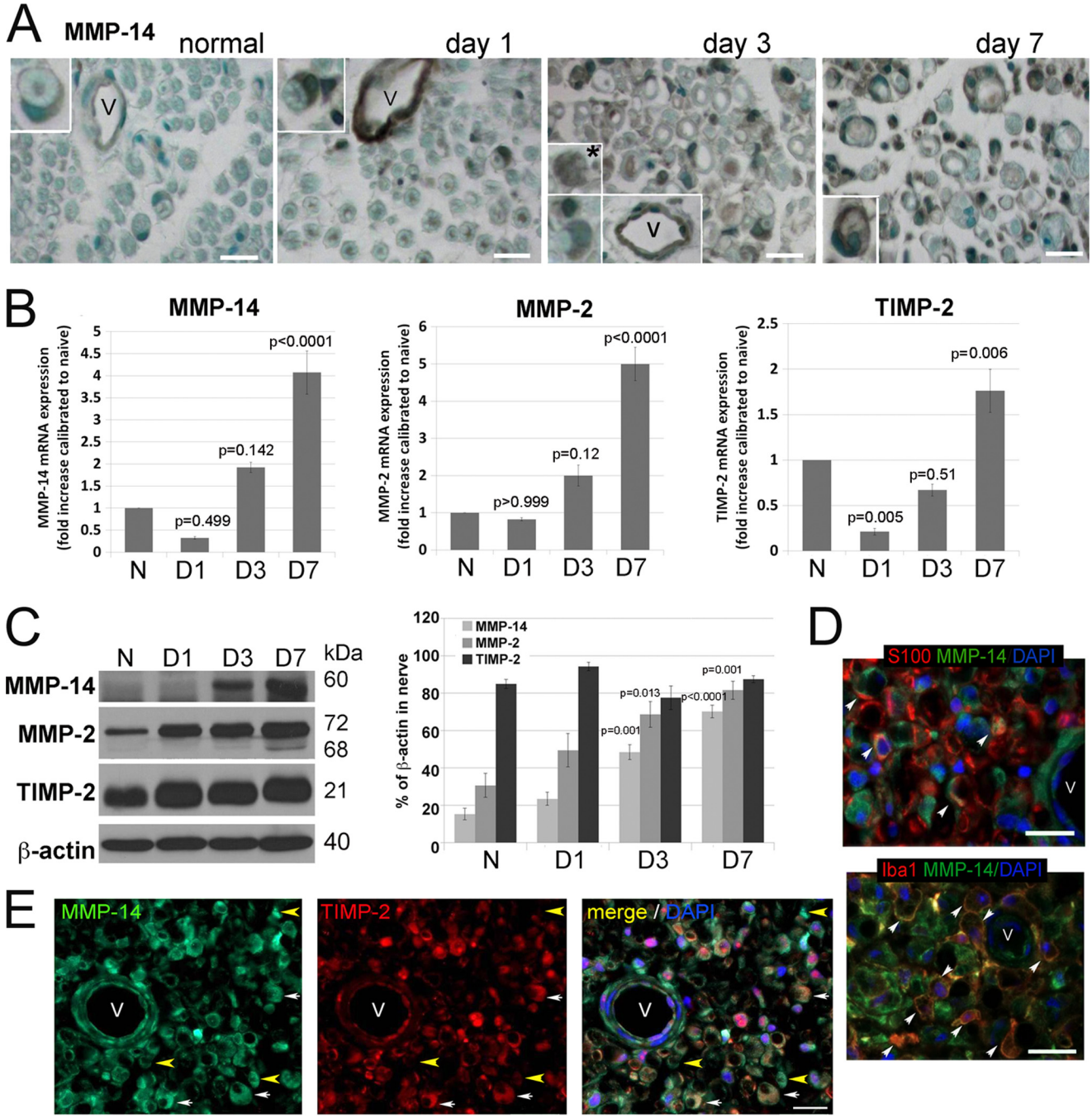


FIGURE 3. **The MMP-14/MMP-2/TIMP-2 axis in the PNS.** *A*, immunostaining for MMP-14 using 3G4 antibody (2′2-diaminobenzidine; *brown*) in rat sciatic nerves at day 0 (normal) and days 1, 3, and 7 after crush injury (the crush site). MMP-14 is observed in Schwann cells (crescent-shaped; *insets*) and vessel (*V*) endothelial cells in all nerves and in macrophage-like cells at day 3 postinjury (*asterisk*). Images are representative of $n = 3$–4/group. *Scale bars* are 25 μm. *B*, TaqMan qPCR of MMP-14, MMP-2, and TIMP-2 in rat sciatic nerves at day 0 (normal (*N*)) and days 1, 3, and 7 after crush injury. The mean relative mRNA of $n = 4$/group are normalized to GAPDH and compared with the normal nerve samples (*p* values by analysis of variance and Bonferroni post hoc test) is shown. *C*, immunoblotting for MMP-14 (60 kDa), MMP-2 (72 and 68 kDa, latent and active, respectively), and TIMP-2 (21 kDa) in rat sciatic nerve at day 0 (normal) and days 1, 3, and 7 after crush injury. The graph represents the mean optical density of $n = 4$/group as a percentage of β-actin (*p* values by analysis of variance and Bonferroni post hoc test). *D*, immunostaining for MMP-14 (3G4 antibody; *green*) in the injured nerve with Schwann cells (S100; *top*, *red*) or macrophages (Iba1; *bottom*, *red*) depicts co-localization of the signals in the injured nerve (*arrowhead*). *E*, immunostaining of MMP-14 (3G4 antibody; *green*) and TIMP-2 (*red*) in rat sciatic nerve at day 3 postcrush. Schwann cells co-express MMP-14 and TIMP-2 (crescent-shaped structures; *white arrows*). TIMP-$2^-$/MMP-$14^+$ structures are observed (*yellow arrowhead*). *D* and *E*, all sections show DAPI-stained nuclei (*blue*) and vessels (*V*). Images are representative of $n = 3$/group. *Scale bars* are 25 μm. *Error bars* represent S.E.

*The MMP-14/MMP-2/TIMP-2 Axis in Schwann Cells in Vitro*—Because Schwann cells are the major source of MMP-14 and TIMP-2 in the nerve, we analyzed their expression and activity levels in the pure Schwann cell cultures. The baseline MMP-14 and TIMP-2 expression levels in the cultured Schwann cells were high (Fig. 4, *A* and *B*). Thus, amplification plots for the MMP-14 and TIMP-2 transcripts show the similar threshold cycle (Ct) values between the normal nerve and cultured Schwann cells (50 ng of cDNA; equal amounts) that closely follow that of the housekeeping *GAPDH* gene (0–5 cycle

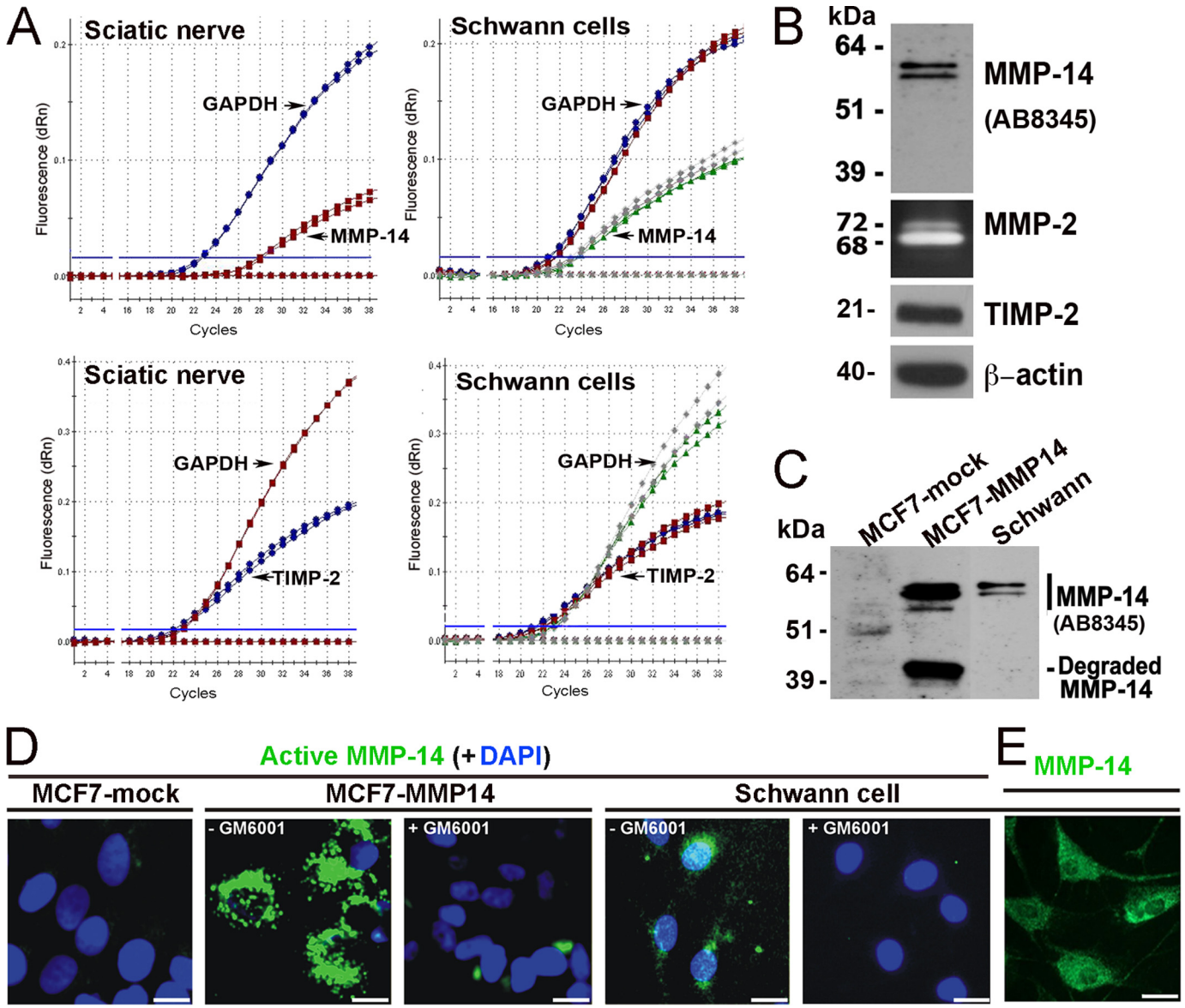


FIGURE 4. **The MMP-14/MMP-2/TIMP-2 axis in Schwann cells *in vitro*.** *A*, TaqMan qPCR amplification plots for MMP-14, TIMP-2, and GAPDH (normalizer) in primary rat Schwann cell cultures (grown in DMEM containing 10% FBS for 24 h) and normal rat sciatic nerve. MMP-14 and TIMP-2 amplification closely follows GAPDH amplification (*i.e.* 0–5 cycle intervals between threshold cycle (Ct) values), suggesting high baseline expression of both the enzyme and its inhibitor. Data shown are from duplicate Schwann cell samples (same color curves) from two independent experiments or duplicate nerve samples (same color curves) pooled from $n = 5$/sample. *B*, immunoblotting for MMP-14 (AB8345 antibody) and TIMP-2 of Schwann whole cell lysate aliquots (5 $\mu$g/lane) and gelatin zymography of the Schwann cell medium aliquots (20 $\mu$l) for the activation status of MMP-2. $\beta$-Actin is used as a loading control. *dRn*, the fluorescence emission of the baseline. *C*, immunoblotting of MMP-14 (AB8345 antibody) in MCF7-mock, MCF7-MMP14, and Schwann cell whole cell lysate aliquots (equal amounts; 3.5 $\mu$g/lane each). *D*, imaging of the catalytically active cellular MMP-14. MCF7-mock, MCF7-MMP14, and Schwann cells were co-incubated for 3 h with the MP-3653 fluorescent reporter alone or jointly with the non-fluorescent hydroxamate inhibitor GM6001 (+*GM6001*). The resulting fluorescence of the cell-bound MP-3653 reporter recorded active MMP-14 (*green*). DAPI stains the nuclei (*blue*). *Scale bars* are 8 $\mu$m. *E*, Schwann cells immunostaining with the MMP-14 3G4 antibody are reactive with both active and inactive enzyme (*green*). *Scale bars* are 15 $\mu$m.

intervals between Ct values; Fig. 4*A*). These data suggest that Schwann cells are both the abundant and the main source of MMP-14 and TIMP-2 in normal PNS.

These data were corroborated by immunoblotting of Schwann cell lysates with MMP-14 and TIMP-2 antibodies (Fig. 4*B*). Gelatin zymography of the conditioned medium aliquots showed both the inactive (72-kDa) and active (68-kDa) MMP-2 enzyme secreted by cultured Schwann cells (Fig. 4*B*).

Given the high levels of both MMP-14 and its inhibitor, TIMP-2, we sought to assess the level of catalytically active, TIMP-2-free MMP-14 in Schwann cells using a selective MP-3653 reporter we described recently (32) and control human breast carcinoma MCF7 cells used frequently in MMP-14 studies (35). Because endogenous expression of both TIMP-2 and MMP-14 in MCF7 cells is exceedingly low, MCF7 cells with forced expression of MMP-14 (MCF7-MMP14) produce high levels of TIMP-2-free MMP-14 (35). As judged by immunoblotting with the polyclonal MMP-14 AB8345 antibody (Fig. 4*C*), rat Schwann cells displayed an approximately severalfold lower level of MMP-14 compared with human MCF7-MMP14 cells. As anticipated, MCF7 cells expressing an empty vector (MCF7-mock) exhibited no detectable MMP-14.

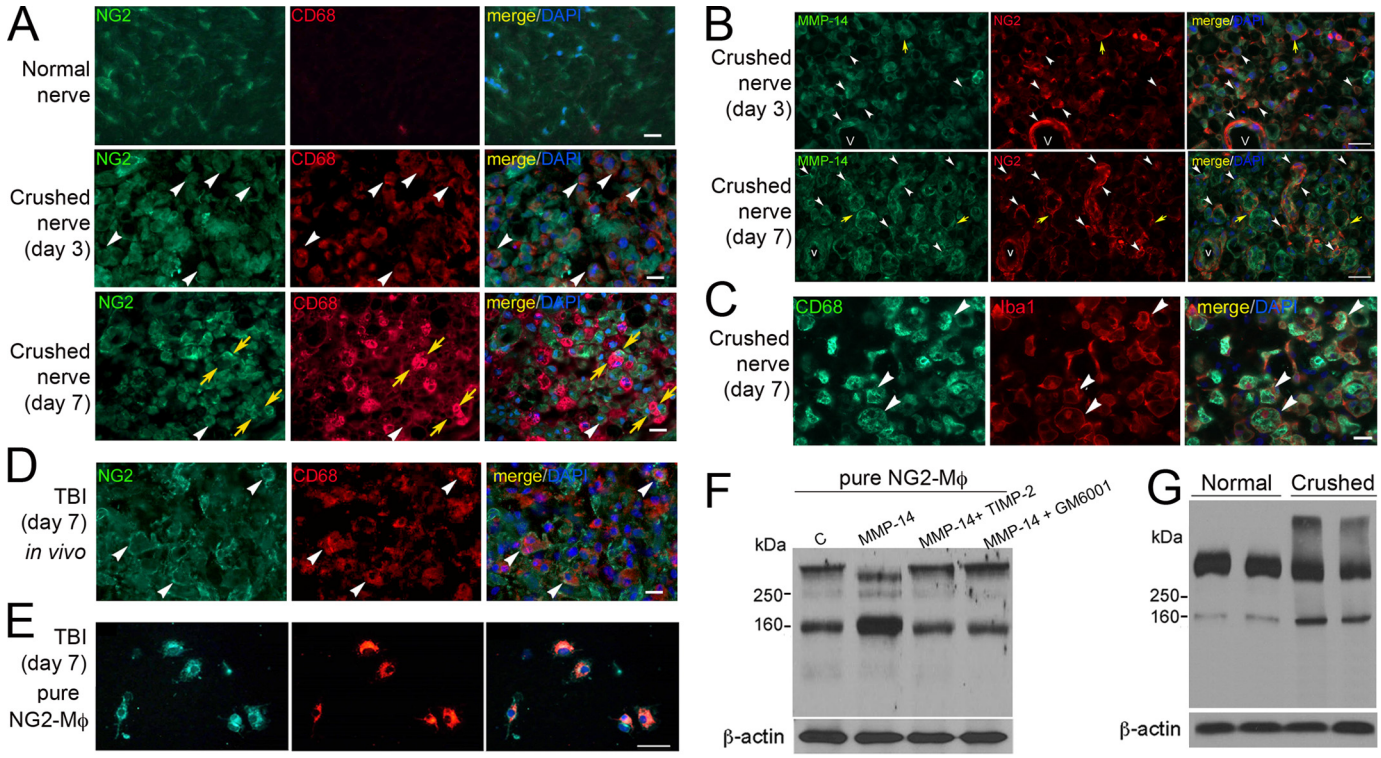


FIGURE 5. **NG2-Mϕ in the PNS and in cultures stimulated with MMP-14.** *A*, immunostaining of NG2 (*green*) and CD68 (*red*) in rat sciatic nerve at day 0 (normal) and days 3 and 7 after crush injury. $NG2^+/CD68^+$ cells (*white arrowheads*) and $NG2^+/CD68^-$ cells adjacent to $NG2^-/CD68^+$ Mϕ (*yellow arrows*) are observed. *Scale bars* are 25 μm. *B*, immunostaining of MMP-14 (3G4 antibody; *green*) and NG2 (AB5320 antibody; *red*) in sciatic nerve at days 3 and 7 postcrush. *White arrowheads*, NG2 co-localized with MMP-14 in fibroblast-like cells and microvascular (*V*) pericytes and/or endothelial cells especially at day 7 postcrush. *Yellow arrows*, MMP-14 and NG2 interface when expressed by adjacent cells. *Scale bars* are 30 μm. *C*, immunostaining of Iba1 (*red*) and CD68 (*green*) in rat sciatic nerve at day 7 postcrush. Macrophages recruited into the injury site are predominantly $CD68^+$ phagocytes. *Scale bars* are 20 μm. *D*, immunostaining of NG2 (AB5320 antibody; *green*) and CD68 (*red*) in the TBI lesion epicenter shows $NG2^+/CD68^+$ cells (*white arrowheads*). *Scale bar* are 20 μm. *A–D*, images are representative of $n = 4$/group. *E*, immunostaining of NG2 (AB5320 antibody; *green*) and CD68 (*red*) in the fixed (4% PFA) NG2-Mϕ cultures isolated from the TBI lesion epicenter from *D*. Images are representative of brain tissues from about $n = 5$/group. *Scale bars* are 25 μm. *A–E*, DAPI stains the nuclei (*blue*). *F*, immunoblotting of NG2 (05-710 antibody) in the cultured NG2-Mϕ lysates from *E*. Where indicated, the cells were incubated with MMP-14 (1 μg/ml) alone or jointly with TIMP-2 (50 ng) or GM6001 (10 μM) for 30 min. Data are representative of two independent experiments with brain tissues from about $n = 5$/group. *G*, immunoblotting of NG2 (05-710 antibody) in sciatic nerve at days 0 (normal) and 7 postcrush. Duplicate representative samples of $n = 4$/group are shown. *F* and *G*, β-actin is used as a loading control.

Because of the presence of the active site zinc ion-interacting inhibitory hydroxamate warhead, the MP-3653 reagent interacts only with the TIMP-2-free active cellular MMP-14 enzyme rather than with the MMP-14 latent zymogen or the inactive stoichiometric TIMP-2·MMP-14 complex (32). In this respect, MP-3653 is similar to GM6001, a hydroxamate inhibitor of MMPs, including MMP-14. In contrast with GM6001, the presence of the fluorescent moiety in MP-3653 allows the direct and quantitative visualization of MP-3653 bound to the cells and accordingly the levels of the active cellular MMP-14 in these cells. Thus, MCF7-MMP14, MCF7-mock, and Schwann cells were co-incubated with MP-3653 alone or jointly with the non-fluorescent GM6001 competitor. As judged by the efficiency of MP-3653 binding to the cells, there was a high level of the active MMP-14 enzyme in MCF7-MMP14 cells and a noticeable, albeit significantly lower, level in Schwann cells (Fig. 4*D*). An exceedingly low MMP-14 level was observed in the original MCF7-mock cells. MP-3653 binding to cellular MMP-14 was competitively eliminated in the presence of GM6001 in both the MCF7-MMP14 and Schwann cells. Schwann cells immunostaining for MMP-14 were used as a positive control (Fig. 4*E*). These data, especially when combined, demonstrate the presence of the catalytically active MMP-14 in Schwann cells.

*NG2-Mϕ Infiltrate the PNS and Utilize MMP-14 to Shed NG2 in Vitro*—In the PNS, NG2 is expressed by endoneurial fibroblasts and microvascular pericytes in both normal and injured nerves (5, 6, 45). In line with these reports, NG2 was detected in the elongated fibroblast-like cells and microvascular pericytes in normal and crushed nerves (Fig. 5, *A* and *B*). NG2 co-localized with MMP-14 in pericytes and macrophage-like cells at both days 3 and 7 postcrush (Fig. 5*B*, *yellow* and *white arrows*). Considering our finding of NG2 reactivity in macrophage-like cells and because hematogenous NG2-Mϕ infiltrate CNS lesions, such as TBI (11–13), we aimed to determine the contribution of NG2-Mϕ to PNS injury.

Hematogenous Mϕ infiltrate the PNS at days 2–7 postcrush to assist in phagocytic clearance of the axonal debris (46, 47). We analyzed the NG2 and CD68 (macrophage marker) co-immunoreactivity in the sciatic nerve samples obtained at day 0 (normal) and days 3 and 7 postcrush (Fig. 5*A*). In normal nerve, the level of CD68-positive Mϕ was limited (Fig. 5*A*). The number of the $NG2^+/CD68^+$ Mϕ infiltrating the nerve increased transiently at day 3 (*white arrows*) and then declined by day 7 postcrush. Instead, NG2-labeled cells adjacent to $NG2^-/CD68^+$ Mϕ were observed at day 7 postcrush (*yellow arrows*). Because CD68-labeled (*i.e.* phagocytic) cells were at both time

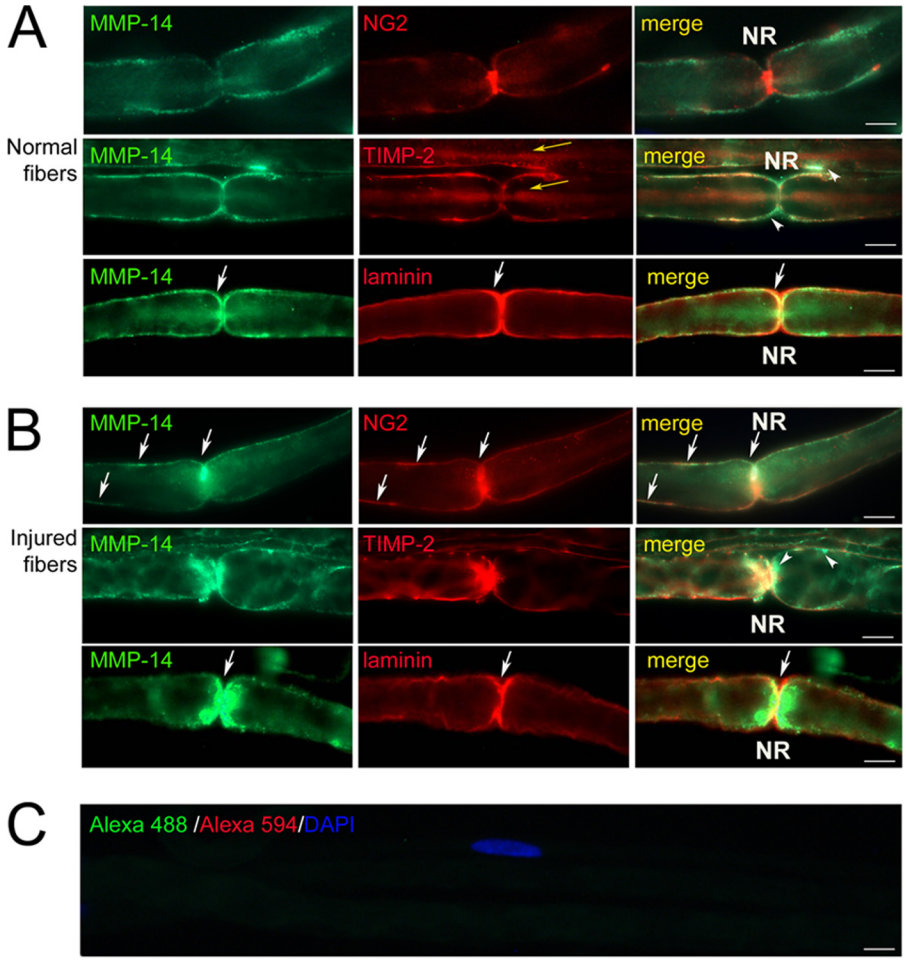


FIGURE 6. **MMP-14 translocation toward the node of Ranvier (*NR*).** Immunostaining of MMP-14 (3G4 antibody; *green*) and NG2 (AB5320 antibody; *red*), TIMP-2 (*red*), or laminin (*red*) in teased out myelinated nerve fibers in rat sciatic nerves at days 0 (normal; *A*) and 3 after transection (*B*) is shown. Control (*C*) is stained using species-specific secondary antibodies conjugated to Alexa Fluor 488 (*green*) and Alexa Fluor 594 (*red*). *White arrows* indicate MMP-14 co-localized with its substrates, NG2 and laminin, postinjury. *White arrowheads* indicate TIMP-2$^{-}$/MMP-14$^{+}$ reactivity. *Yellow arrows* indicate intraaxonal TIMP-2 staining. Images are representative of ~40/group. *Scale bars* are 5 $\mu$m.

points totally cross-reactive with Iba1, a general macrophage marker (Fig. 5*C*), we concluded that NG2-M$\phi$ co-expressed both CD68 and Iba1 in the PNS.

As a positive control, we used the samples obtained from the brain lesion at day 7 after TBI (12). The NG2 membrane immunoreactivity was largely associated with M$\phi$ in our positive control day 7 TBI brain samples (Fig. 5*D*), consistent with the previous studies.

Because NG2 was sensitive to MMP-14 proteolysis, we next evaluated the role of MMP-14 proteolysis of NG2 in NG2-M$\phi$ *in vitro*. Because the required quantities of NG2-M$\phi$ are not available from the injured nerve source, the primary NG2-M$\phi$ cultures were isolated from the TBI lesion according to established protocols (11–13). According to the results of NG2 and CD68 immunostaining, over 90% of the cultured cells represented NG2-M$\phi$ (Fig. 5*E*). The purified NG2-M$\phi$ were co-incubated with MMP-14 alone or jointly with TIMP-2 or GM6001 for 24 h, then lysed, and analyzed by NG2 immunoblotting (Fig. 5*F*). The intact 300- and 160-kDa NG2 species were detected in the untreated NG2-M$\phi$. In the presence of MMP-14, the 300-kDa NG2 was transformed into the major 290- and minor 260–275-kDa species concomitantly with a significant increase in the 160-kDa NG2. According to the earlier data, the 290- and 260–275-kDa species represent the shed soluble and shed membrane NG2, respectively (18, 37). In the presence of TIMP-2 or GM6001, MMP-14 proteolysis of NG2 was fully repressed. These data suggested that exogenously added MMP-14 was capable of shedding NG2 expressed in the infiltrating NG2-M$\phi$.

Consistent with the previous reports (5, 6, 45) and our findings in the primary NG2-M$\phi$ cultures, immunoblotting analysis identified two NG2 species, the 300-kDa major and 160-kDa minor species, in normal nerve (Fig. 5*G*). In the crushed nerve samples (day 7), the levels of the 160-kDa NG2 species increased significantly with a concomitant decrease in the 300-kDa intact NG2 potentially due to the proteolysis of NG2 following nerve injury. In contrast to NG2-M$\phi$ cultures, an additional, very high molecular weight NG2 band was detected in the crushed nerve samples (Fig. 5*G*). This band was also observed by others and identified as an NG2 species containing multiple, additional glycosaminoglycan chains (5). Together, our data documented the transient expression of NG2 by a subpopulation of infiltrating M$\phi$ in the damaged PNS (within 3 days postinjury) in a pattern distinct from that in CNS lesions

and suggested that NG2 in NG2-M$\phi$ was susceptible to MMP-14 proteolysis.

*MMP-14 Translocation in Myelinated Fibers*—Next, we assessed the relative changes in MMP-14, its substrates (NG2 and laminin), and TIMP-2 using immunofluorescence staining of the individually teased myelinated fibers (Fig. 6). To confirm the analyses of the injured fibers, the nerves were transected; there was no apparent difference in the staining profiles between the proximal and distal stumps.

In the normal nerve (Fig. 6*A*), the MMP-14 immunoreactivity was observed in the Schwann cell plasma and/or basement membrane, structures that are not distinguishable without using electron microscopy. In agreement with the earlier reports (5, 45), NG2 was localized in the Schwann cell basement membrane (5, 6, 45) and the nodes of Ranvier (45) of the uninjured fibers. Partial co-localization of the TIMP-2 immunoreactivity with that of MMP-14 was also noted. TIMP-2 was also observed intra-axonally. Laminin displayed its specialized and characteristic Schwann cell basement membrane distribution.

In the nerve at day 3 postinjury (Fig. 6*B*), there was a significant translocation of both MMP-14 and TIMP-2 toward the paranodal/nodal areas where the MMP-14 immunoreactivity only partially co-localized with TIMP-2. Whereas NG2 and laminin staining remained in the same structures, these substrates co-localized with the MMP-14 enzyme in close proximity to the nodes of Ranvier uniquely and only following nerve injury (Fig. 6*B*). For each antigen, the staining specificity was confirmed using the non-immune serum or by omission of the primary antibody (Fig. 6*C*). These novel data evidence the injury-specific translocation of MMP-14 in close proximity to its substrate, such as NG2, at the nodes of Ranvier.

*Selective and Short Term Inhibition of MMP-14 Accelerates Axon Regeneration*—To test further the importance of MMP-14 in nerve injury, we used the human MMP-14 DX2400 antibody (28). In contrast with the broad spectrum synthetic MMP inhibitors, this function-blocking antibody does not cross-react with other MMPs (48). Because of the 98–99% homology between human and rat catalytic domain sequences of MMP-14, DX2400 was suitable in our system. The schedule we used to identify the effect of DX2400 is illustrated in Fig. 7*A*. Specifically, at day 3 postcrush, rats received a single intraneural injection of DX2400. PBS (vehicle) and human IgG1 were used as controls.

First, a von Frey test was done 5 days before day 0 (baseline) and then at days 3 (before the injection), 5, and 7 postcrush to assess the sensory behavioral recovery in rats that received vehicle or DX2400. Both animal groups developed a similar heightened sensitivity to innocuous tactile stimulation at day 3 postcrush as evident by the reduced threshold of paw withdrawal (Fig. 7*B*). A single injection of DX2400 at day 3 reversed the established hypersensitivity to tactile stimulation (measured at days 5 and 7) relative to the vehicle group. As expected, contralateral to injury, hind paws in both groups showed no change in mechanical sensitivity (Fig. 7*B*). Neither the vehicle nor IgG1 alone affected sensory behavioral recovery (data not shown).

Next, regeneration of the sensory axons was measured using a nerve pinch test at day 7 postcrush (Fig. 7, *C* and *D*). The regeneration distance (the distance between the crush site and the distal nerve site responsive to pinch testing; Fig. 7*C*) was $12 \pm 0.89$, $12.7 \pm 0.44$, and $17.1 \pm 0.61$ mm with PBS, IgG1, and DX2400, respectively, suggesting that axons regenerated with an average speed of 2.43 mm/day after a single DX2400 injection compared with 1.7 mm/day after injection of the controls (Fig. 7*D*). These data indicated that highly selective MMP-14 inhibition increased the speed of sensory nerve regrowth by roughly 40%. We then excised two 10-mm-long consecutive nerve segments distal to the crush/injection site and the segmental L4/L5 DRG from these rats for additional molecular analyses.

In agreement with the nerve pinch test, the immunoblotting data for cAMP-dependent transcription factor 3 (ATF3), which is required for activation of the regenerative transcriptional program in DRG neurons after PNS injury (40), revealed increased ATF3 levels in DRG ipsilateral to sciatic nerve crush at day 7 postcrush for the DX2400 treatment compared with the IgG1 or PBS treatment. Because PBS and IgG1 groups showed comparable data, only the latter is presented henceforth. As expected, in both groups, the ATF3 expression was elevated in the ipsilateral compared with the contralateral DRG (Fig. 7*E*, *Norm*). These data were corroborated by qPCR analysis of the DRG samples that showed a $14.8 \pm 1.8$-fold increase ($p = 0.049$) in the relative ATF3 mRNA at day 7 postcrush in the ipsilateral compared with the contralateral DRG in the control and a 23.8- $\pm$ 3.3-fold increase in the DX2400 group ($n = 3–4$/group).

GAP-43, a marker of regenerative axon growth (40), considerably increased in crushed nerve segments A and B compared with the contralateral normal nerve (Fig. 7*F*). In addition, the relative GAP-43 levels in segment A exceeded that of segment B in the DX2400 samples relative to the IgG1 samples. According to immunostaining of the comparable segments (Fig. 7*G*), DX2400 caused a roughly 3-fold increase in GAP-43 when compared with IgG1. These GAP-43 immunoreactivity data precisely correlate with the length of regenerating axons after DX2400 and IgG1 therapy in each segment as observed by pinch testing (Fig. 7*D*). Similarly to GAP-43, MMP-14 inhibition by DX2400 resulted in an approximately 2.5-fold increase in NG2 and laminin, the targets of MMP-14 proteolysis. Together, these data demonstrate that selective, short term local inhibition of the MMP-14 activity facilitates regeneration of sensory neurons and reverses the established mechanical hypersensitivity after PNS injury.

## DISCUSSION

The present study reveals for the first time that MMP-14/MT1-MMP 1) is an efficient and unique NG2 sheddase; 2) sheds NG2 on NG2-M$\phi$, which infiltrate the PNS after injury; 3) is present in the PNS both as the inactive stoichiometric TIMP-2·MMP-14 complex and the active enzyme; 4) translocates toward the nodes of Ranvier and such substrates as NG2 postinjury; and 5) can be selectively inhibited to enhance sensory axonal growth and reverse the established hypersensitivity in the rat PNS injury model.

Individual MMPs have both detrimental and beneficial effects in the PNS. In general, broad spectrum MMP inhibition

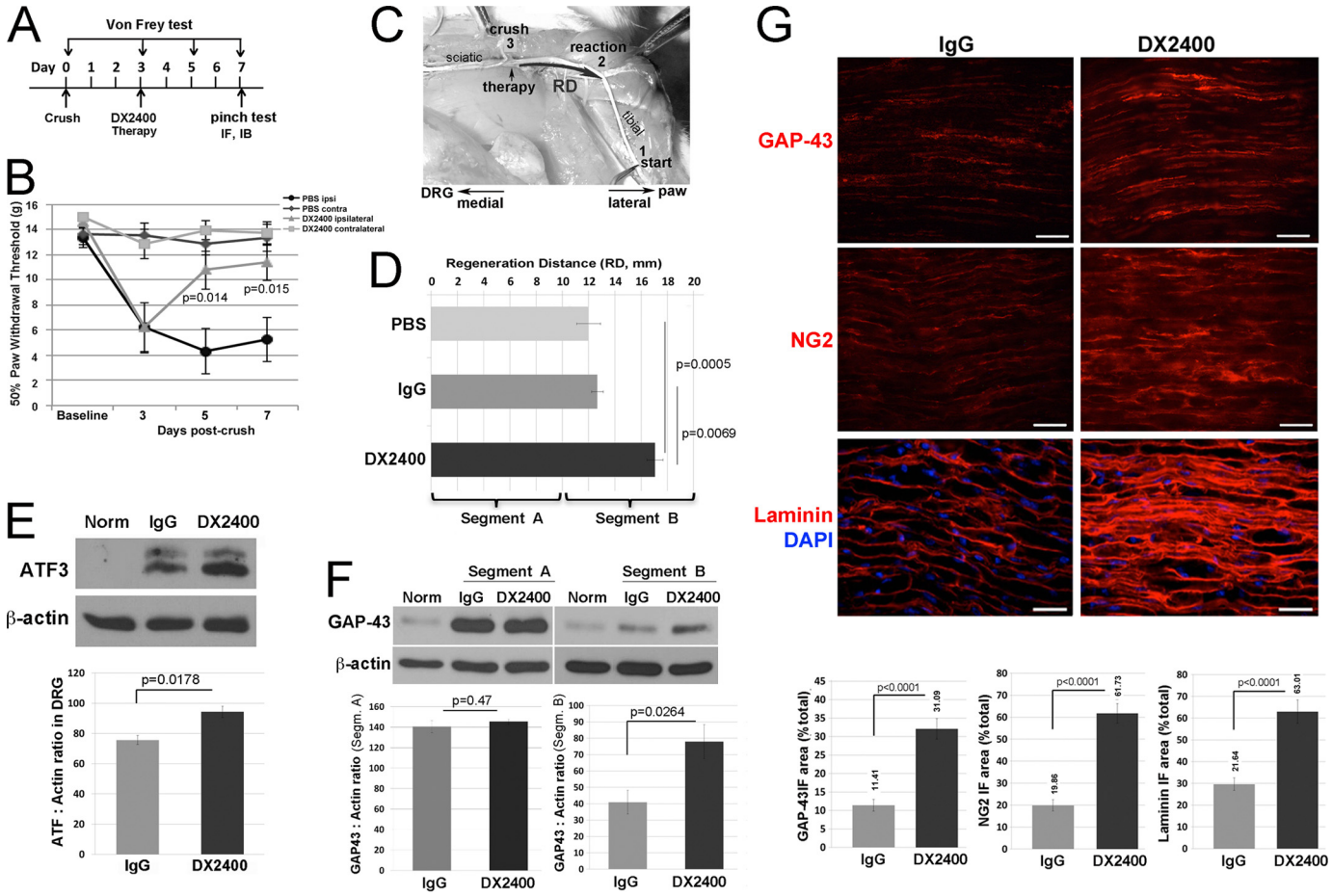


FIGURE 7. **Function-blocking human MMP-14 antibody (DX2400) enhanced axon regeneration in the PNS.** *A*, experimental schedule of the intraneural administration of DX2400 (1.1 mg/ml), control human IgG1 (1.1 mg/ml), or PBS alone (5 $\mu$l each) into rat sciatic nerve (crush site) once at day 3 postcrush. von Frey testing was done at days −5, −3, −1, 0, 3, 5, and 7 postcrush. Sensory axon regeneration was assessed by a nerve pinch test at day 7 postcrush followed by immunostaining (*IF*) or immunoblotting (*IB*) analyses at day 7 postcrush. *B*, MMP-14 inhibition reversed mechanical hypersensitivity as assessed by von Frey testing as described in *A*. The mean withdrawal threshold (gram-force; *g*) of $n = 10$/group (*p* values by Student's *t* test) is shown. *C*, an illustration of a nerve pinch test in rats is shown in the dorsal plane. The exposed sciatic nerve and its tibial branch are pinched with forceps in 1-mm-long consecutive segments starting from the distal end of the tibial nerve (*1*), proceeding in the proximal direction until a reflex response is observed. The distance between the reaction site (*2*) and the crush site (*3*) is defined as the regeneration distance (*RD*). *D*, MMP-14 inhibition increased the speed of sensory nerve regrowth. The mean regeneration distance (mm) of $n = 5$–8/group increased after treatment with DX2400 compared with control IgG1 or PBS (*p* values by analysis of variance and Bonferroni post hoc test). The 10-mm nerve segments at and immediately distal to the crush/injection site (0–10 mm; segment A) and consecutively distal (10–20 mm; segment B) were analyzed. *E*, MMP-14 inhibition increased intraganglionic ATF3. Immunoblotting of ATF3 in L4/L5 DRG at day 7 postcrush and after therapy described in *A* contralateral to nerve crush after IgG1 treatment (*Norm*) and ipsilateral to nerve crush after control IgG1 or DX2400 treatment. $\beta$-Actin is used as a loading control. The graph represents the mean ATF3 to actin ratio of $n = 5$/group (*p* value by Student's *t* test). *F*, immunoblotting of GAP-43 in the nerve samples contralateral to nerve crush after IgG1 treatment (*Norm*) and in the injured nerve segments (*Segm.*) A and B after control IgG1 and DX2400 treatment described in *D*. $\beta$-Actin is used as a loading control. The graph represents the mean GAP-43 to actin ratio of $n = 4$/group (*p* value by Student's *t* test). *G*, immunostaining of GAP-43, NG2 (AB5320 antibody), and laminin (*red* for each) in sciatic nerve after IgG1 or DX2400 injection at day 7 postcrush as described in *A*. DAPI stains nuclei (*blue*). *Scale bars* are 40 $\mu$m. The graphs represent the mean immunofluorescence (*IF*) area as a percentage of total area of $n = 5$/group (*p* value by Student's *t* test). *Error bars* represent S.E.

promotes sensory axon regeneration by stimulating Schwann cell mitosis (19), limiting axonal dieback (49), and preventing release of the inhibitory myelin-associated glycoprotein residues (50). Likewise, MMP inhibition attenuates pain associated with PNS injury by preventing the MMP-9- and MMP-2-mediated release of algesic cytokines and myelin basic protein (21–23). According to our data, brief, local MMP-14 inhibition by a highly selective function-blocking antibody mimics these pro-regenerative and analgesic effects of broad spectrum MMP inhibition (19). MMP-14 inhibition enhanced the speed of sensory axon regrowth at least in part by preserving growth-permissive laminin (17, 51) from degradation and promoting the intraganglionic expression of ATF3 and GAP-43. Conceptually, the present data are consistent with a model in which a misbalance in the MMP-9/TIMP-1 axis, inducible early in PNS injury by inflammatory stimulants (*e.g.* LPS and TNF$\alpha$), or in the MMP-14/MMP-2/TIMP-2 axis, constitutive and inducible later in PNS injury, contributes to axonal and myelin damage, neuroinflammation, and pain (19–24, 52).

MMP-14 performs as an efficient and unconventional NG2 sheddase with the cleavage sites localized in the N-terminal D1 domain of NG2. This is in contrast with several MMPs and ADAMs (a disintegrin and metalloproteinases) that proteolyze NG2 at the D3 domain (18, 37, 43). In general, our results confirm and expand the earlier observations that cleavage of a shed ~260–275-kDa membrane-tethered NG2 species in NG2-expressing cells is selectively inhibited by TIMP-2 (18, 37). MMP-14 cleavage at the D1 domain may not alter NG2 binding

to collagen IV, PDGF, or basic FGF, which is ascribed to the D2 or D3 domains (36). In NG2-M$\phi$, MMP-14 released an additional ~290-kDa fragment, which was determined in the earlier works by others to be a soluble full-length ectodomain shed at a juxtamembrane site (18, 37); hence, this proteolytic process cannot be effectively analyzed using the purified NG2 ectodomain. Together, these data suggest that, in contrast to other MMPs/ADAMs, MMP-14 cleavages occur within the N-terminal D1 domain and then stimulate additional cleavages in the D3 domain, including those by other proteases, resulting in both the shed soluble and shed membrane NG2 species.

The node of Ranvier is the key structure in both the generation of action potential (53) and initiation of the axonal growth sprouts (1). After nerve injury, a fraction of the MMP-14 enzyme was redistributed toward the nodes of Ranvier. This finding makes plausible the proposed models of nodal NG2 shedding as a potential regulator of axonal conduction (54) and axonal growth (45). However, NG2 functions in axon growth remain highly controversial because of evidence of its inhibitory role (55–57) and the permissive functions of NG2-expressing cells (58, 59). Although the functions of the individual NG2 species cannot be effectively studied in a global NG2 deletion model, overall NG2 was concluded not to be essential to PNS regeneration or neuropathic pain (60). Importantly, our study clearly shows a correlation between the proregenerative traits of MMP-14 inhibition and the accumulation of the NG2 immunoreactivity in the PNS. However, our study does not directly demonstrate a putative link between MMP-14 proteolysis of NG2 and axon regeneration.

In PNS, NG2 is known to associate with the Schwann cell basement membrane and the nodes of Ranvier (5, 6, 45). These earlier studies demonstrated that soluble NG2 was predominantly present in the PNS and suggested that fibroblasts, rather than Schwann cells, deposited NG2 into the Schwann cell basement membrane, although others believe that non-myelinating Schwann cells express NG2 in response to injury (61, 62). Considerable quantities of the very high molecular weight glycosylated NG2 species present in the nerve specifically postinjury (5) are not observed in cultured NG2-M$\phi$. Conversely, MMP-14 sheds NG2 species in NG2-M$\phi$, which are present only transiently in the damaged PNS.

NG2-M$\phi$ infiltrate the PNS at 3 days after crush injury, implying transient NG2 expression by a subpopulation of infiltrating M$\phi$. Although little is known about the functions of NG2-M$\phi$ in the damaged PNS, it is apparent that this cell type expresses both CD68 and Iba1 in the PNS and that NG2-M$\phi$ isolated from CNS lesions express growth factors and display neuroprotective properties (12, 13). This suggestion correlates with the established M$\phi$ function in governance of Wallerian degeneration, phagocytic debris clearance, and generation of a permissive milieu for axon growth in the PNS (46, 47, 63). However, given that multiple M$\phi$ phenotypes may exist, the outcomes of NG2 expression or proteolysis of NG2 in M$\phi$ in the PNS remain obscure. It is interesting to note that, due to the prevention of M$\phi$ attack of growth cones, inactivation of MMP-9 promotes DRG axonal growth cultured on inhibitory CSPG-1/aggrecan (49). Although NG2 and the MMP/TIMP axis both regulate proliferation and migration of NG2-glia of the CNS, MMP-14 proteolysis could have diversified effects on NG2 function in various cells (*e.g.* M$\phi$, fibroblasts, and pericytes) of the PNS.

In summary, our findings implicate MMP-14 as a novel protease that cleaves NG2 and a promising drug target for improved peripheral nerve repair. We have provided the first evidence in the nervous system for the therapeutic potential of the selective, function-blocking human MMP-14 antibody (DX2400). By protecting permissive substrates (*e.g.* laminin) from degradation, suppressing the algesic action of MMP-2 (21), and stimulating the regenerative program in the sensory neurons, the selective, local, and short term inhibition of MMP-14 activity promoted axonal growth and reversed the established hypersensitivity arising from PNS damage. Caution, however, is required in developing the sustained or late stage MMP-14 inhibitor therapy as this therapy may also target certain functions that are beneficial to nerve repair, such as the MMP-2-mediated degradation of inhibitory CSPGs (25, 26) and myelination (20, 64, 65).

## REFERENCES


1. Chen, Z. L., Yu, W. M., and Strickland, S. (2007) Peripheral regeneration. *Annu. Rev. Neurosci.* **30,** 209–233
2. Busch, S. A., and Silver, J. (2007) The role of extracellular matrix in CNS regeneration. *Curr. Opin. Neurobiol.* **17,** 120–127
3. Fawcett, J. W. (2006) Overcoming inhibition in the damaged spinal cord. *J. Neurotrauma* **23,** 371–383
4. Nishiyama, A., Komitova, M., Suzuki, R., and Zhu, X. (2009) Polydendrocytes (NG2 cells): multifunctional cells with lineage plasticity. *Nat. Rev. Neurosci.* **10,** 9–22
5. Morgenstern, D. A., Asher, R. A., Naidu, M., Carlstedt, T., Levine, J. M., and Fawcett, J. W. (2003) Expression and glycanation of the NG2 proteoglycan in developing, adult, and damaged peripheral nerve. *Mol. Cell. Neurosci.* **24,** 787–802
6. Rezajooi, K., Pavlides, M., Winterbottom, J., Stallcup, W. B., Hamlyn, P. J., Lieberman, A. R., and Anderson, P. N. (2004) NG2 proteoglycan expression in the peripheral nervous system: upregulation following injury and comparison with CNS lesions. *Mol. Cell. Neurosci.* **25,** 572–584
7. Stallcup, W. B. (2002) The NG2 proteoglycan: past insights and future prospects. *J. Neurocytol.* **31,** 423–435
8. Kucharova, K., Chang, Y., Boor, A., Yong, V. W., and Stallcup, W. B. (2011) Reduced inflammation accompanies diminished myelin damage and repair in the NG2 null mouse spinal cord. *J. Neuroinflammation* **8,** 158
9. de Castro, R., Jr., Tajrishi, R., Claros, J., and Stallcup, W. B. (2005) Differential responses of spinal axons to transection: influence of the NG2 proteoglycan. *Exp. Neurol.* **192,** 299–309
10. Onda, A., Yabuki, S., Kikuchi, S., Satoh, K., and Myers, R. R. (2001) Effects of lidocaine on blood flow and endoneurial fluid pressure in a rat model of herniated nucleus pulposus. *Spine* **26,** 2186–2191
11. Matsumoto, H., Kumon, Y., Watanabe, H., Ohnishi, T., Shudou, M., Chuai, M., Imai, Y., Takahashi, H., and Tanaka, J. (2008) Accumulation of macrophage-like cells expressing NG2 proteoglycan and Iba1 in ischemic core of rat brain after transient middle cerebral artery occlusion. *J. Cereb. Blood Flow Metab.* **28,** 149–163
12. Nishihara, T., Ochi, M., Sugimoto, K., Takahashi, H., Yano, H., Kumon, Y., Ohnishi, T., and Tanaka, J. (2011) Subcutaneous injection containing IL-3 and GM-CSF ameliorates stab wound-induced brain injury in rats. *Exp. Neurol.* **229,** 507–516
13. Smirkin, A., Matsumoto, H., Takahashi, H., Inoue, A., Tagawa, M., Ohue, S., Watanabe, H., Yano, H., Kumon, Y., Ohnishi, T., and Tanaka, J. (2010) $Iba1^+/NG2^+$ macrophage-like cells expressing a variety of neuroprotective factors ameliorate ischemic damage of the brain. *J. Cereb. Blood Flow Metab.* **30,** 603–615
14. Jones, L. L., Yamaguchi, Y., Stallcup, W. B., and Tuszynski, M. H. (2002)

NG2 is a major chondroitin sulfate proteoglycan produced after spinal cord injury and is expressed by macrophages and oligodendrocyte progenitors. *J. Neurosci.* **22,** 2792–2803
15. Bu, J., Akhtar, N., and Nishiyama, A. (2001) Transient expression of the NG2 proteoglycan by a subpopulation of activated macrophages in an excitotoxic hippocampal lesion. *Glia* **34,** 296–310
16. Nagase, H., Visse, R., and Murphy, G. (2006) Structure and function of matrix metalloproteinases and TIMPs. *Cardiovasc. Res.* **69,** 562–573
17. Page-McCaw, A., Ewald, A. J., and Werb, Z. (2007) Matrix metalloproteinases and the regulation of tissue remodelling. *Nat. Rev. Mol. Cell Biol.* **8,** 221–233
18. Asher, R. A., Morgenstern, D. A., Properzi, F., Nishiyama, A., Levine, J. M., and Fawcett, J. W. (2005) Two separate metalloproteinase activities are responsible for the shedding and processing of the NG2 proteoglycan in vitro. *Mol. Cell. Neurosci.* **29,** 82–96
19. Liu, H., Kim, Y., Chattopadhyay, S., Shubayev, I., Dolkas, J., and Shubayev, V. I. (2010) MMP inhibition enhances the rate of nerve regeneration in vivo by promoting de-differentiation and mitosis of supporting Schwann cells. *J. Neuropathol. Exp. Neurol.* **69,** 386–395
20. Kim, Y., Remacle, A. G., Chernov, A. V., Liu, H., Shubayev, I., Lai, C., Dolkas, J., Shiryaev, S. A., Golubkov, V. S., Mizisin, A. P., Strongin, A. Y., and Shubayev, V. I. (2012) The MMP-9/TIMP-1 axis controls the status of differentiation and function of myelin-forming Schwann cells in nerve regeneration. *PLoS One* **7,** e33664
21. Kawasaki, Y., Xu, Z. Z., Wang, X., Park, J. Y., Zhuang, Z. Y., Tan, P. H., Gao, Y. J., Roy, K., Corfas, G., Lo, E. H., and Ji, R. R. (2008) Distinct roles of matrix metalloproteases in the early- and late-phase development of neuropathic pain. *Nat. Med.* **14,** 331–336
22. Liu, H., Shiryaev, S. A., Chernov, A. V., Kim, Y., Shubayev, I., Remacle, A. G., Baranovskaya, S., Golubkov, V. S., Strongin, A. Y., and Shubayev, V. I. (2012) Immunodominant fragments of myelin basic protein initiate T cell-dependent pain. *J. Neuroinflammation* **9,** 119
23. Kobayashi, H., Chattopadhyay, S., Kato, K., Dolkas, J., Kikuchi, S., Myers, R. R., and Shubayev, V. I. (2008) MMPs initiate Schwann cell-mediated MBP degradation and mechanical nociception after nerve damage. *Mol. Cell. Neurosci.* **39,** 619–627
24. Shubayev, V. I., Angert, M., Dolkas, J., Campana, W. M., Palenscar, K., and Myers, R. R. (2006) TNFα-induced MMP-9 promotes macrophage recruitment into injured peripheral nerve. *Mol. Cell. Neurosci.* **31,** 407–415
25. Krekoski, C. A., Neubauer, D., Graham, J. B., and Muir, D. (2002) Metalloproteinase-dependent predegeneration *in vitro* enhances axonal regeneration within acellular peripheral nerve grafts. *J. Neurosci.* **22,** 10408–10415
26. Zuo, J., Ferguson, T. A., Hernandez, Y. J., Stetler-Stevenson, W. G., and Muir, D. (1998) Neuronal matrix metalloproteinase-2 degrades and inactivates a neurite-inhibiting chondroitin sulfate proteoglycan. *J. Neurosci.* **18,** 5203–5211
27. Hughes, P. M., Wells, G. M., Perry, V. H., Brown, M. C., and Miller, K. M. (2002) Comparison of matrix metalloproteinase expression during Wallerian degeneration in the central and peripheral nervous systems. *Neuroscience* **113,** 273–287
28. Devy, L., Huang, L., Naa, L., Yanamandra, N., Pieters, H., Frans, N., Chang, E., Tao, Q., Vanhove, M., Lejeune, A., van Gool, R., Sexton, D. J., Kuang, G., Rank, D., Hogan, S., Pazmany, C., Ma, Y. L., Schoonbroodt, S., Nixon, A. E., Ladner, R. C., Hoet, R., Henderikx, P., Tenhoor, C., Rabbani, S. A., Valentino, M. L., Wood, C. R., and Dransfield, D. T. (2009) Selective inhibition of matrix metalloproteinase-14 blocks tumor growth, invasion, and angiogenesis. *Cancer Res.* **69,** 1517–1526
29. Shiryaev, S. A., Cieplak, P., Aleshin, A. E., Sun, Q., Zhu, W., Motamedchaboki, K., Sloutsky, A., and Strongin, A. Y. (2011) Matrix metalloproteinase proteolysis of the mycobacterial HSP65 protein as a potential source of immunogenic peptides in human tuberculosis. *FEBS J.* **278,** 3277–3286
30. Chen, E. I., Li, W., Godzik, A., Howard, E. W., and Smith, J. W. (2003) A residue in the S2 subsite controls substrate selectivity of matrix metalloproteinase-2 and matrix metalloproteinase-9. *J. Biol. Chem.* **278,** 17158–17163
31. Knight, C. G. (1995) Active-site titration of peptidases. *Methods Enzymol.* **248,** 85–101
32. Remacle, A. G., Shiryaev, S. A., Golubkov, V. S., Freskos, J. N., Brown, M. A., Karwa, A. S., Naik, A. D., Howard, C. P., Sympson, C. J., and Strongin, A. Y. (2013) Non-destructive and selective imaging of the functionally active, pro-invasive membrane type-1 matrix metalloproteinase (MT1-MMP) enzyme in cancer cells. *J. Biol. Chem.* **288,** 20568–20580
33. Tanaka, J., Toku, K., Matsuda, S., Sudo, S., Fujita, H., Sakanaka, M., and Maeda, N. (1998) Induction of resting microglia in culture medium devoid of glycine and serine. *Glia* **24,** 198–215
34. Brockes, J. P., Fields, K. L., and Raff, M. C. (1979) Studies on cultured rat Schwann cells. I. Establishment of purified populations from cultures of peripheral nerve. *Brain Res.* **165,** 105–118
35. Rozanov, D. V., Deryugina, E. I., Ratnikov, B. I., Monosov, E. Z., Marchenko, G. N., Quigley, J. P., and Strongin, A. Y. (2001) Mutation analysis of membrane type-1 matrix metalloproteinase (MT1-MMP). The role of the cytoplasmic tail $Cys^{574}$, the active site $Glu^{240}$, and furin cleavage motifs in oligomerization, processing, and self-proteolysis of MT1-MMP expressed in breast carcinoma cells. *J. Biol. Chem.* **276,** 25705–25714
36. Tillet, E., Ruggiero, F., Nishiyama, A., and Stallcup, W. B. (1997) The membrane-spanning proteoglycan NG2 binds to collagens V and VI through the central nonglobular domain of its core protein. *J. Biol. Chem.* **272,** 10769–10776
37. Nishiyama, A., Lin, X. H., and Stallcup, W. B. (1995) Generation of truncated forms of the NG2 proteoglycan by cell surface proteolysis. *Mol. Biol. Cell* **6,** 1819–1832
38. Nishiyama, A., Dahlin, K. J., Prince, J. T., Johnstone, S. R., and Stallcup, W. B. (1991) The primary structure of NG2, a novel membrane-spanning proteoglycan. *J. Cell Biol.* **114,** 359–371
39. Livak, K. J., and Schmittgen, T. D. (2001) Analysis of relative gene expression data using real-time quantitative PCR and the $2^{-\Delta\Delta CT}$ method. *Methods* **25,** 402–408
40. Seijffers, R., Mills, C. D., and Woolf, C. J. (2007) ATF3 increases the intrinsic growth state of DRG neurons to enhance peripheral nerve regeneration. *J. Neurosci.* **27,** 7911–7920
41. McQuarrie, I. G., Grafstein, B., and Gershon, M. D. (1977) Axonal regeneration in the rat sciatic nerve: effect of a conditioning lesion and of dbcAMP. *Brain Res.* **132,** 443–453
42. Chaplan, S. R., Bach, F. W., Pogrel, J. W., Chung, J. M., and Yaksh, T. L. (1994) Quantitative assessment of tactile allodynia in the rat paw. *J. Neurosci. Methods* **53,** 55–63
43. Larsen, P. H., Wells, J. E., Stallcup, W. B., Opdenakker, G., and Yong, V. W. (2003) Matrix metalloproteinase-9 facilitates remyelination in part by processing the inhibitory NG2 proteoglycan. *J. Neurosci.* **23,** 11127–11135
44. Strongin, A. Y., Collier, I., Bannikov, G., Marmer, B. L., Grant, G. A., and Goldberg, G. I. (1995) Mechanism of cell surface activation of 72-kDa type IV collagenase. Isolation of the activated form of the membrane metalloprotease. *J. Biol. Chem.* **270,** 5331–5338
45. Martin, S., Levine, A. K., Chen, Z. J., Ughrin, Y., and Levine, J. M. (2001) Deposition of the NG2 proteoglycan at nodes of Ranvier in the peripheral nervous system. *J. Neurosci.* **21,** 8119–8128
46. Perry, V. H., Brown, M. C., and Gordon, S. (1987) The macrophage response to central and peripheral nerve injury. A possible role for macrophages in regeneration. *J. Exp. Med.* **165,** 1218–1223
47. Kieseier, B. C., Hartung, H. P., and Wiendl, H. (2006) Immune circuitry in the peripheral nervous system. *Curr. Opin. Neurol.* **19,** 437–445
48. Devy, L., and Dransfield, D. T. (2011) New strategies for the next generation of matrix-metalloproteinase inhibitors: selectively targeting membrane-anchored MMPs with therapeutic antibodies. *Biochem. Res. Int.* **2011,** 191670
49. Busch, S. A., Horn, K. P., Silver, D. J., and Silver, J. (2009) Overcoming macrophage-mediated axonal dieback following CNS injury. *J. Neurosci.* **29,** 9967–9976
50. Milward, E., Kim, K. J., Szklarczyk, A., Nguyen, T., Melli, G., Nayak, M., Deshpande, D., Fitzsimmons, C., Hoke, A., Kerr, D., Griffin, J. W., Calabresi, P. A., and Conant, K. (2008) Cleavage of myelin associated glycoprotein by matrix metalloproteinases. *J. Neuroimmunol.* **193,** 140–148
51. Luckenbill-Edds, L. (1997) Laminin and the mechanism of neuronal outgrowth. *Brain Res. Brain Res. Rev.* **23,** 1–27
52. Chattopadhyay, S., and Shubayev, V. I. (2009) MMP-9 controls Schwann

cell proliferation and phenotypic remodeling via IGF-1 and ErbB receptor-mediated activation of MEK/ERK pathway. *Glia* **57,** 1316–1325
53. Poliak, S., and Peles, E. (2003) The local differentiation of myelinated axons at nodes of Ranvier. *Nat. Rev. Neurosci.* **4,** 968–980
54. Hunanyan, A. S., García-Alías, G., Alessi, V., Levine, J. M., Fawcett, J. W., Mendell, L. M., and Arvanian, V. L. (2010) Role of chondroitin sulfate proteoglycans in axonal conduction in mammalian spinal cord. *J. Neurosci.* **30,** 7761–7769
55. Fidler, P. S., Schuette, K., Asher, R. A., Dobbertin, A., Thornton, S. R., Calle-Patino, Y., Muir, E., Levine, J. M., Geller, H. M., Rogers, J. H., Faissner, A., and Fawcett, J. W. (1999) Comparing astrocytic cell lines that are inhibitory or permissive for axon growth: the major axon-inhibitory proteoglycan is NG2. *J. Neurosci.* **19,** 8778–8788
56. Ughrin, Y. M., Chen, Z. J., and Levine, J. M. (2003) Multiple regions of the NG2 proteoglycan inhibit neurite growth and induce growth cone collapse. *J. Neurosci.* **23,** 175–186
57. Tan, A. M., Colletti, M., Rorai, A. T., Skene, J. H., and Levine, J. M. (2006) Antibodies against the NG2 proteoglycan promote the regeneration of sensory axons within the dorsal columns of the spinal cord. *J. Neurosci.* **26,** 4729–4739
58. Busch, S. A., Horn, K. P., Cuascut, F. X., Hawthorne, A. L., Bai, L., Miller, R. H., and Silver, J. (2010) Adult NG2+ cells are permissive to neurite outgrowth and stabilize sensory axons during macrophage-induced axonal dieback after spinal cord injury. *J. Neurosci.* **30,** 255–265
59. Yang, Z., Suzuki, R., Daniels, S. B., Brunquell, C. B., Sala, C. J., and Nishiyama, A. (2006) NG2 glial cells provide a favorable substrate for growing axons. *J. Neurosci.* **26,** 3829–3839
60. Hossain-Ibrahim, M. K., Rezajooi, K., Stallcup, W. B., Lieberman, A. R., and Anderson, P. N. (2007) Analysis of axonal regeneration in the central and peripheral nervous systems of the NG2-deficient mouse. *BMC Neurosci.* **8,** 80
61. Jones, L. L., Sajed, D., and Tuszynski, M. H. (2003) Axonal regeneration through regions of chondroitin sulfate proteoglycan deposition after spinal cord injury: a balance of permissiveness and inhibition. *J. Neurosci.* **23,** 9276–9288
62. Schneider, S., Bosse, F., D'Urso, D., Muller, H., Sereda, M. W., Nave, K., Niehaus, A., Kempf, T., Schnolzer, M., and Trotter, J. (2001) The AN2 protein is a novel marker for the Schwann cell lineage expressed by immature and nonmyelinating Schwann cells. *J. Neurosci.* **21,** 920–933
63. Brück, W. (1997) The role of macrophages in Wallerian degeneration. *Brain Pathol.* **7,** 741–752
64. Lehmann, H. C., Köhne, A., Bernal, F., Jangouk, P., Meyer Zu Hörste, G., Dehmel, T., Hartung, H. P., Previtali, S. C., and Kieseier, B. C. (2009) Matrix metalloproteinase-2 is involved in myelination of dorsal root ganglia neurons. *Glia* **57,** 479–489
65. Court, F. A., Zambroni, D., Pavoni, E., Colombelli, C., Baragli, C., Figlia, G., Sorokin, L., Ching, W., Salzer, J. L., Wrabetz, L., and Feltri, M. L. (2011) MMP2–9 cleavage of dystroglycan alters the size and molecular composition of Schwann cell domains. *J. Neurosci.* **31,** 12208–12217